Please cite this article in press as: Wang et al., Creep-Enabled 3D Solid-State Lithium-Metal Battery, Chem (2020), https://doi.org/10.1016/j.chempr.2020.09.005

Chem

CellPress

Perspective

Creep-Enabled 3D Solid-State Lithium-Metal Battery

Ziqiang Wang,[1] Xiaoyan Li,[2,*] Yuming Chen,[1,2,*] Kai Pei,[1] Yiu-Wing Mai,[3] Sulin Zhang,[4,*] and Ju Li[1,*]

SUMMARY

Existing all-solid-state Li-metal batteries suffer attacks by the chemically aggressive and mechanically stressful Li metal. Li metal is a soft crystal and may exhibit either displacive or diffusive deformation. Here, we describe a class of all-solid-state Li-metal batteries enabled by 3D porous Li-metal hosts made of electrochemically stable mixed Li-ion and electronic conductor (MIEC) and electronic and Li-ion insulators (ELI). Within 3D open porous MIEC/ELI structure, Li metal advances and retracts via interfacial diffusional creep as an "incompressible working fluid" with fast stress relaxation and minimal contact with a solid electrolyte (SE), thereby significantly improving the electrochemomechanical stability. *In situ* transmission electron microscopy corroborated with thermodynamic analyses offers design principles in materials, sizes, and interfaces of the 3D porous MIEC/ELI structures, which are applicable to other alkali-metal batteries. The successful construction of a creep-enabled battery engine opens a new avenue toward high-density, electrochemically and mechanically robust all-solid-state Li-metal batteries.

INTRODUCTION

The ever-increasing demand for safe and dense energy storage with particular applications to electric vehicles and power grids has shifted the scientific research from organic liquid electrolyte based Li-ion batteries (LIBs) toward all-solid-state batteries.[1] Among all the anode substitutes for LIBs, Li metal is the most attractive candidate due to its very low electrochemical potential and very high theoretical specific capacity. In addition to the enhanced energy density,[2] a major advantage of all-solid-state Li-metal battery is the potential increase in safety by avoiding the use of volatile and flammable liquid electrolytes.[3] Considering that Li metal is a soft crystal, the all-solid construction also holds the potential for suppressing Li-dendrite formation, thereby increasing the cycling life.[4] Furthermore, recent success in the development of solid electrolytes (SEs) with ionic conductivities comparable with that of the liquid electrolytes makes high-power-density all-solid-state Li-metal batteries possible.[5]

Despite the great potential and significant progress in all-solid-state Li-metal batteries, several entangled challenges remain, preventing Li-metal batteries from becoming a viable technology: Li metal is a solid, yet it is required to change shape and grow over a long range without generating much local stress during Li deposition and stripping; Li metal is both chemically corrosive and mechanically stressful to surrounding solid components, yet the deforming Li metal needs to maintain uninterrupted electronic and ionic contacts with the SE and current collector (M), respectively. These scientific challenges are further detailed below.

The Bigger Picture

Challenges and opportunities:

- Existing all-solid-state Li-metal battery suffers a series of attacks by the chemically aggressive and mechanically stressful Li metal, which significantly limits the cycle life of the Li-metal batteries
- All-solid-state Li-metal battery engine featuring a 3D porous Li-metal host is constructed, which can activate the diffusional creep of Li metal for fast stress relaxation on the one hand and suppress the corrosive reactions for improved electrochemical stability on the other
- These findings resolve the entangled electrochemical and mechanical instabilities and open a new design paradigm for electrochemically friendly and mechanically robust all-solid-state batteries with superior energy density and long cyclability

Please cite this article in press as: Wang et al., Creep-Enabled 3D Solid-State Lithium-Metal Battery, Chem (2020), https://doi.org/10.1016/j.chempr.2020.09.005

Fracture of Solid Electrolytes by Dendrite Penetration

Li-metal deposition requires extra volume around the deposition sites, which can, in principle, generate large mechanical stress driven by a small overpotential according to the Nernst equation. The electrochemically generated mechanical stresses will then be transmitted to surrounding solid components that can crack the SEs and lead to Li-metal penetration through the SEs (Figure 1A),[6] and subsequently shorting the battery. Based on the linear elasticity theory, Monroe and Newman predicted that morphological instability of a flat Li/SE interface can be mechanically suppressed provided that the shear modulus of the SEs is over two times higher than that of the Li metal.[7] However, contrary to this prediction, it was found that Li dendrites can still grow into stiff SEs (e.g., $Li_7La_3Zr_2O_{12}$ (LLZO))[8–13] even though the shear modulus of LLZO (~60 GPa[14]) is one order of magnitude higher than that of Li metal (~1.6 GPa[15]). The Monroe-Newman theory[7] failed because it assumes perfect, defect-free SE that is chemically stable (phase stable) against Li_{BCC} and purely elastic Li metal. In reality, preexisting flaws are inevitable in SEs, and these defects are favorite sites for Li plating. Under the applied overpotential, the displacive Li deposition into the defects generates large stress, which may drive the formation of Griffith cracks. Continuous Li deposition into the crack is kinetically favored, forming Li dendrite on the one hand and wedging Griffith crack propagation on the other, along either grain boundaries or intragranular pathways.[8] Noticeably, stress relaxation through dislocation-mediated plasticity (yielding) is not effective since plastic yielding can only be activated at a very high stress level for small-scale metals.[16] Diffusion mediated creep is a more favored pathway for stress relaxation, which has been demonstrated for nanoscale Ag at room temperature.[17,18] The electrochemically induced mechanical stress, if not relaxed quickly, could fracture the SEs. Thus, stress relaxation is the first priority if one wants to prevent shorting of the battery and thermal runaway hazards.

Electrochemical Stability at the Interface

Li metal is chemically corrosive. Almost all SEs of high Li-ion conductivities are thermodynamically prone to decomposition against Li metal.[19] This is in itself not a fatal issue provided that the formed solid-electrolyte interphase (SEI) is stable (indeed, this is how the graphite anode in conventional LIB works). The main problem is how to keep the SEI stably in contact with the moving/expanding/shrinking Li metal without falling off. During electrochemical cycling, mechanical agitation concomitant with the morphological changes may spall the solid SEI off from the SEs into debris. This would cause continuous consumption of active Li and uncontrollable SEI growth on the one hand and blockage of the electronic percolation pathway on the other due to the electronically insulating SEI debris (Figure 1A).

Maintaining Contact with Moving Li Metal

Despite that Li metal is both chemically corrosive and mechanically stressful, the moving Li metal must maintain constant electronic and ionic contact with the current collector and the SE, respectively. In liquid cells, the fluidity of liquid electrolytes endows continuous ionic paths. Whereas in all-solid-state batteries, maintaining contact between the SEs and the moving Li metal, with both being solids, becomes a significant challenge. For two-dimensional (2D) Li-foil anodes, the relative volumetric change during Li deposition and stripping is virtually infinite (from zero to finite), surpassing any other anodes including Si (300% volume increase). Although a 2D Li metal foil can start out fully dense and cohesive to the SEs, it is unrealistic to expect that the SEs can accommodate such a drastic morphological change by following the moving Li metal for a distance of tens of microns without fracture or interfacial delamination (Figure 1A).[20–23] Indeed, the loss of interfacial adhesion

[1]Department of Nuclear Science and Engineering and Department of Materials Science and Engineering, Massachusetts Institute of Technology, Cambridge, MA 02139, USA

[2]College of Environmental Science and Engineering, Fujian Normal University, Fuzhou 350007, China

[3]Centre for Advanced Materials Technology (CAMT), School of Aerospace, Mechanical and Mechatronics Engineering J07, The University of Sydney, Sydney, NSW 2006, Australia

[4]Department of Engineering Science and Mechanics, The Pennsylvania State University, University Park, PA 16802, USA

*Correspondence: xiaoyanli1985@126.com (X.L.), yumingc126@126.com (Y.C.), suz10@psu.edu (S.Z.), liju@mit.edu (J.L.)

https://doi.org/10.1016/j.chempr.2020.09.005

Please cite this article in press as: Wang et al., Creep-Enabled 3D Solid-State Lithium-Metal Battery, Chem (2020), https://doi.org/10.1016/j.chempr.2020.09.005

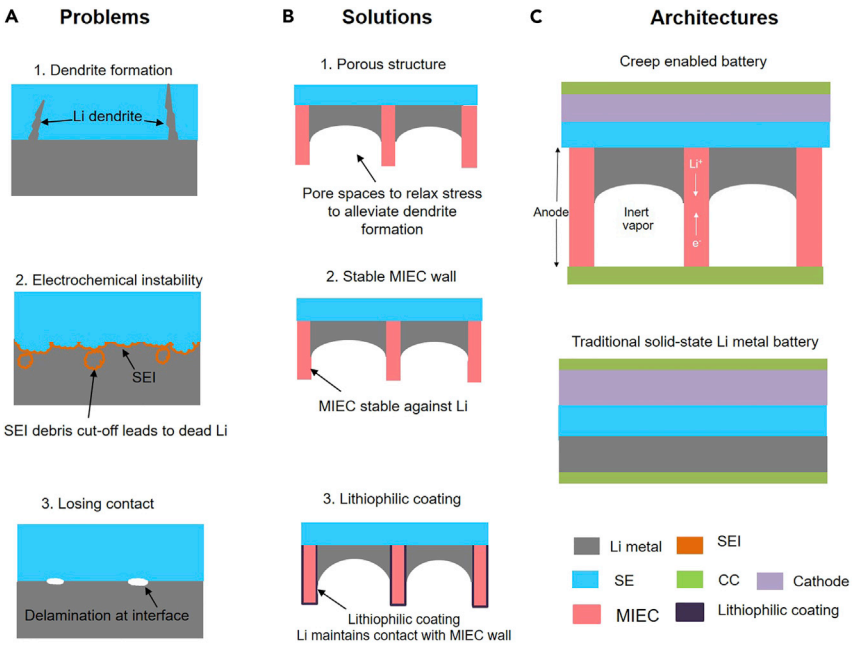

Figure 1. Schematic of Designs and Problems of Battery

(A) Current problems for the solid-state lithium-metal battery.

(B) Designs and solutions provided by the design of the creep-enabled 3D solid-state lithium-metal battery.

(C) The architecture of creep-enabled 3D solid-state lithium-metal battery, in comparison with the traditional solid-state lithium-metal battery with the layered "sandwich" architecture.

has been frequently observed experimentally,[24–26] and identified as one of the major concerns for the capacity decay of all-solid-state Li-metal batteries.

These challenges have been extremized in the development of the all-solid-state rechargeable Li-metal batteries with the traditional 2D sandwich architecture (Figure 1C). The current strategy for solving these problems centers on improving the performance of SEs, such as through increasing the ductility of the SEs, chemical doping, surface defects reduction, etc.[27–29] This strategy, however, can only partially solve the issues from a phase stability and theoretical mechanics perspective. In this paper, we review a promising design strategy for the battery engine in which Li metal is engineered as a "creeping fluid," just as the working fluid in mechanical engines.[16,30–33] Distinct from the previous constructions focusing on the SEs, the creeping Li metal in the battery engine is in minimal contact with SEs, but mainly with the 3D host made of mixed Li-ion and electronic conductor (MIEC) and electronic and Li-ion insulators (ELI) that are thermodynamically stable in direct contact with Li metal (Figure 1C). If confined in the diffusive creep regime, Li metal in the battery engine can advance and retract without causing much stress, while the MIEC/ELI mediated interfaces direct robust electronic and ionic pathways as well as cut-offs for Li deposition and stripping. To construct such a chemically and mechanically durable battery engine, we explore material innovation, geometrical design, and interfacial engineering of the MIEC/ELI host. Such a 3D porous architecture resolves the coupled electrochemomechanical instabilities and shows great potential to enable the practical applications of all-solid-state Li-metal batteries.

MATERIALS AND ARCHITECTURES

A novel concept to combat the electrochemomechanical instabilities is to construct a 3D stable Li-metal host with suppressed corrosive reactions and fast stress

Please cite this article in press as: Wang et al., Creep-Enabled 3D Solid-State Lithium-Metal Battery, Chem (2020), https://doi.org/10.1016/j.chempr.2020.09.005

relaxations. While many host materials have been attempted, it has been demonstrated that the MIEC/ELI host in a 3D tubular, or more generally, open porous nano-architecture exhibits superior performance. These two additional classes of materials, along with the classical battery components, SEs (electron insulator but Li-ion conductor) and metals (electron conductor but Li-ion insulator), constitute a complete material space in terms of the electronic/ionic/atomic transport properties. Such an expanded library of materials enables the construction of various interfaces required in the battery engine for directing electronic, ionic, and atomic flows with minimal mechanical stress and moving contact.

The MIEC chosen should be electrochemically stable against the Li metal. This means that MIEC sits on a direct tie-line with Li_{BCC} phase in the bulk equilibrium phase diagram without any intervening phases (Figure 2C). To maintain "staying on" the Li_{BCC}-MIEC tie-line during electrochemical cycling, the cut-off voltage should be kept below the plateau voltage for Li extraction from the MIEC material itself. That is, if the particular MIEC is a lithiated end-member phase in contact with Li_{BCC} on the phase diagram, the absolute anode potential should be kept below a threshold potential that would cause delithiation of this end-member phase. By judiciously choosing the cycling voltage cutoff, the MIEC phase can thus stay dimensional unchanging and phase stable during electrochemical cycling. The same phase stability and voltage cutoff selection criterion holds for ELI binders that mechanically bind the MIEC with SE.

We believe nanoporous MIEC is essential for alleviating stress generation during Li deposition. In a 3D tubular, or more generally, open porous architecture (Figure 1C), the porous channels function as electrochemically stable "rails" that guide the Li-metal flow. The reserved pore spaces in tubules can help relax the accumulated mechanical stresses during Li deposition. As Li deposition may occur not only at the SE/Li_{BCC} interface but also the MIEC/Li_{BCC} interface, the displacive deformations that agitate the spallation of SEIs and drives SE cracking are alleviated. Meanwhile, diffusive motion of neutralized Li atoms (after the charge-transfer reaction Li^{+}(SE) + e^{-}(M,MIEC) = Li) along the MIEC/Li_{BCC} interface can be activated for fast stress relaxation (see Mechanisms). Taken together, the use of open porous MIEC can help suppress dendrite penetrations and Griffith crack extension across the SEs (Figure 1B) and reduce mechanical agitation of the SEIs formed at the SE/Li_{BCC} interface.

The use of MIEC also minimizes the corrosive effect of Li metal. As the MIEC pores guide the flow of Li metal in the third dimension, they ensure that most of the moving Li_{BCC} are in contact with the MIEC walls, instead of the SE, as in the classical solid-state battery setting. Since the MIEC is selected to be thermodynamically stable against the Li metal, Li deposition/stripping can, thus, cycle without producing any SEI at the Li_{BCC}/MIEC interface, a major factor that often leads to capacity loss and performance degradation in hostless Li-metal batteries (Figure 1B). It should be noted that SEI still forms at the SE/Li_{BCC} interface. However, since the MIEC wall warrants smooth Li-ion and electron transport, any fractured or spalling SEI debris inside the tubule cannot cut off the Li-ion and electron percolation to generate dead Li, as shown in the schematic (Figure 2A).

To enhance mechanical stability, MIEC needs to be firmly rooted into the SE. If MIEC nakedly interfaces the SE, neutralized Li would flood toward the fixed MIEC root, causing MIEC/SE interfacial decohesion as Li_{BCC} formed at the interface is very soft. To address this "soft root" problem, a layer of lithiophobic ELI can be terminally coated onto the MIEC. The ELI layer functions as an inert "mechanical binder" between the MIEC wall and the SE. The MIEC/ELI interface and the ELI/SE interface (together they replace

Please cite this article in press as: Wang et al., Creep-Enabled 3D Solid-State Lithium-Metal Battery, Chem (2020), https://doi.org/10.1016/j.chempr.2020.09.005

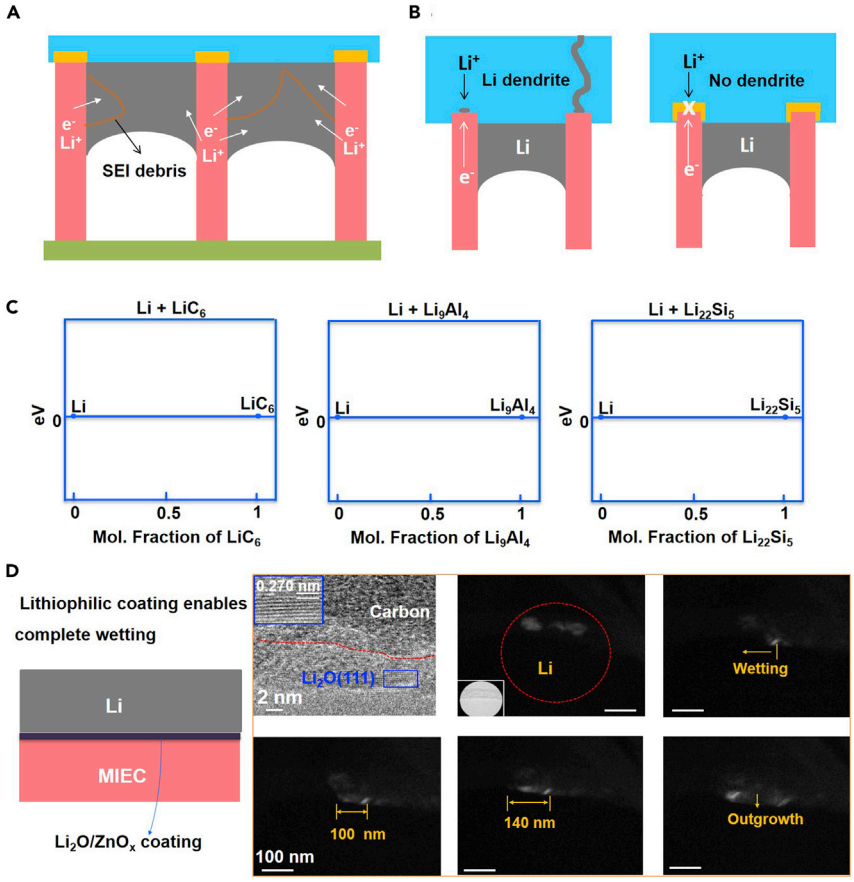

Figure 2. The Advantage of MIEC and Mechanism of Lithiophilicity

(A) The spalling SEI debris inside the tubule cannot cut off the Li-ion and electronic percolation to generate dead lithium.

(B) The ELI material works as an "inert" binder between SE and MIEC walls to prevent dendrite formation and penetration at MIEC roots.

(C) MIECs of LiC_6, $Li_{22}Si_5$, and Li_9Al_4 have a direct tie-line to the Li_{BCC} phase on the equilibrium phase diagram without intervening phases so that they are electrochemically stable against Li metal.

(D) The ZnO_x/Li_2O layer on MIEC surface helps to induce a strong lithiophilicity, as confirmed by the *in situ* TEM observation of the complete wetting of Li along the surface. Reprinted with permission from Chen et al.[30] Copyright 2020 Springer Nature.

the MIEC/SE interface) must both have strong adhesion strength at room temperature such that the MIEC is rooted firmly into the SE all the time during electrochemical cycling. Materials like BeO and SrF_2, which have a large band gap (>4.0 eV) and are thermodynamically stable against Li_{BCC}, belong to ELIs (Pei, K. and Li, J., unpublished data). Materials that have a poor ionic conductivity and are electronic insulators can also be approximated as ELIs (e.g., LiPON with lower Li-ion conductivity in some cases[30]). As the ELI electronically and ionically separates the MIEC wall from the SE, the presence of the ELI layer inhibits nucleation and segregation of soft Li_{BCC} at the root of MIEC, thereby maintaining strong root adhesion between them and suppressing the interfacial corrosive decohesion between the MIEC root and SE layer (Figure 2B).

MECHANISMS

To understand the underlying mechanisms as to how MIEC alleviates the stress and corrosive effects, *in situ* TEM characterizations have been performed using lithiated

Please cite this article in press as: Wang et al., Creep-Enabled 3D Solid-State Lithium-Metal Battery, Chem (2020), https://doi.org/10.1016/j.chempr.2020.09.005

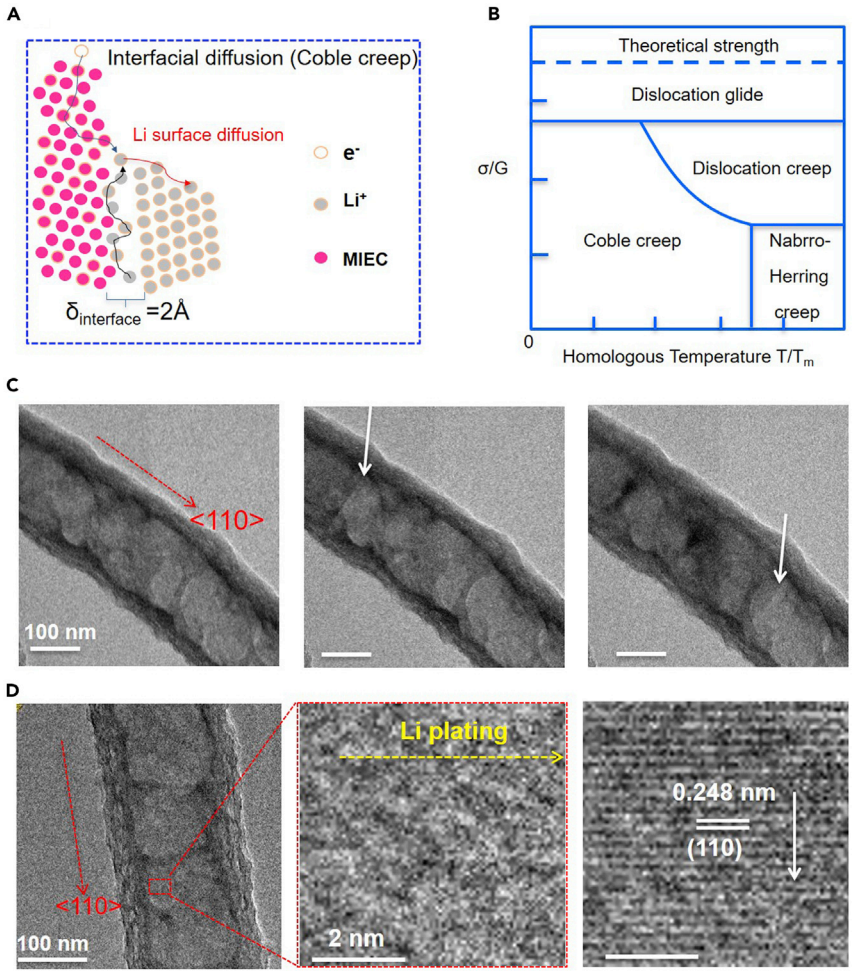

Figure 3. The Mechanism of Li Deposition and Stripping

(A) Schematic for the mechanism of Coble creep that transports via interfacial diffusion along the MIEC/Li_{BCC} incoherent interface. Reprinted with permission from Chen et al.[30] Copyright 2020 Springer Nature.

(B) Schematic of the deformation mechanism map.

(C) TEM images of the Li-metal deposition inside the carbon tubule as a single crystal. Reprinted with permission from Chen et al.[30] Copyright 2020 Springer Nature.

carbon tubules (with a diameter smaller than 200 nm) as the MIEC.[30] Several important observations are highlighted below.

(1) The Li metal can advance and retract inside 3D MIEC channels as a single crystal (Figure 3C) with the body-centered cubic (BCC) atomic structure.
(2) The MIEC tubules allow reversible Li_{BCC} metal deposition/stripping inside across a distance of many microns for 100 cycles, while maintaining excellent structural integrity. The moving Li metal always maintains contact with the MIEC walls, and no dead Li was observed.
(3) Li_{BCC} can continue to plate/strip inside MIEC tubules filled with obstacles or partial obstructions. Moreover, Li stripping can still proceed in the presence of a void plug between the residual Li metal and the SE, suggesting that Li is extracted through the MIEC wall or surface.

Please cite this article in press as: Wang et al., Creep-Enabled 3D Solid-State Lithium-Metal Battery, Chem (2020), https://doi.org/10.1016/j.chempr.2020.09.005

From a theoretical mechanics perspective,[17,33,34,35] the "liquid-like" behavior of crystalline solids, as observed for the Li metal, can be referenced to the definition of the diffusional viscosity of solid by Herring.[36] Viscosity was a terminology reserved for describing the proportionality between stress and strain rate for Newtonian fluids. However, if diffusive mass action in a solid is significant compared with displacive deformation, the solid may change its shape much like a viscous fluid. Li metal at room temperature has a homologous temperature of $T/T_M = 0.66$. Hence, Li metal should exhibit appreciable diffusional creep and be considered as viscous in the low-stress limit.The Li_{BCC} may function as an "incompressible working fluid" that flows inside the MIEC tubules, driven by the overpotential and the mechanical pressure gradient.

Several creep mechanisms exist for metals. The creep strain rate $\dot{\varepsilon}(T,\sigma)$ of Li metal could possibly be driven by the dislocation creep (power-law creep) or diffusional creep (linear creep), according to the deformation mechanism map of metals (Figure 3B). If diffusional creep mechanisms, either the lattice-diffusional Nabarro-Herring creep or interfacial/surface-diffusional Coble creep, are operative, then $\dot{\varepsilon}(T,\sigma) \propto \sigma$, the viscosity η would depend on T and grain size, but not on σ, and Li metal would behave like a Newtonian fluid. On the other hand, if dislocation creep (power-law creep) is operative, then $\eta \propto \sigma^{1-n}$ with $n > 1$, and Li metal would behave like a shear-thinning, non-Newtonian fluid.

Among the competitions between interfacial diffusional Coble creep ($n = 1$), bulk diffusional Nabarro-Herring creep ($n = 1$), and hybrid diffusive-displacive dislocation creep ($n = 3$ to 10) mechanisms, the *in situ* TEM observations have excluded dislocation creep and bulk diffusional Nabarro-Herring creep in the Li-metal bulk as the dominant mechanism. Dislocation creep is excluded by the observation of continuous advance of Li_{BCC} by overcoming partial obstructions inside the tubules during deposition. Both dislocation creep and bulk diffusional Nabarro-Herring creep are excluded by the observation of Li_{BCC} stripping across a void region, since both mechanisms necessitate the presence of bulk Li_{BCC} to accommodate bulk diffusion or bulk dislocation slip. This follows that neutralized Li atoms transport either in the MIEC wall or along the MIEC/Li_{BCC} interface.

Quantitative calculations were carried out to confirm the dominant mechanism.[37,38] For the diffusional creep, there are three possible Li diffusion pathways: (1) via the MIEC wall of width ~10 nm; (2) via the interface between an MIEC wall and Li_{BCC}, with the atomic width of $\delta_{interface}$ (~2 Å); and (3) via bulk Li_{BCC} with width ~100 nm. To understand the mechanism for more general MIEC materials, three canonical MIECs—LiC_6, $Li_{22}Si_5$, and Li_9Al_4 were considered. The calculations were performed with the quantitative estimations of the Li conductivities using the Nernst-Einstein equation for different paths and different MIEC materials. For all the cases, the diffusion flux along the 2-Å incoherent interface between the MIEC and the Li metal (path b) dominates over flux through the 10-nm MIEC wall or through the 100-nm Li-metal bulk. In other words, Li transport along the MIEC is dominated by the Coble creep along the 2-Å interfacial channel, as illustrated in Figure 3A. This realization greatly liberates the material choices available for the MIEC, as long as it can form an incoherent interface with Li_{BCC}.

Incidentally, based on our previous *in situ* TEM study,[17] not only Li, but other metallic elements like Ag could diffuse rapidly along $\delta_{interface}$ ~2 Å interfaces at room temperature, which could explain the behavior of nanoscale Ag in the open porous MIEC buffer layer in a most recent advance in all-solid-state Li-metal batteries.[39]

Please cite this article in press as: Wang et al., Creep-Enabled 3D Solid-State Lithium-Metal Battery, Chem (2020), https://doi.org/10.1016/j.chempr.2020.09.005

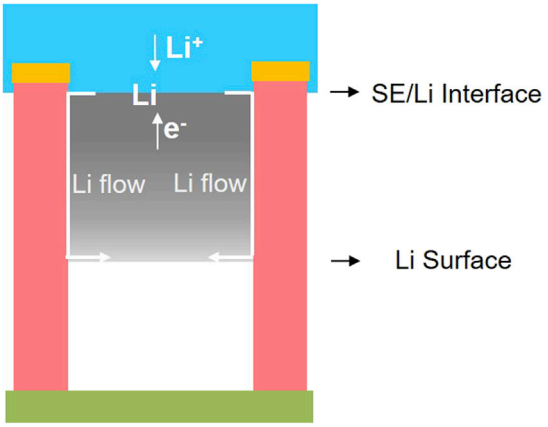

Figure 4. Schematic of the Li Flow and the Pressure Difference on Li Metal in the MIEC Tubule (as Indicated by the Contrast Gradient) during Li-Metal Deposition Process

A lithiophilic MIEC wall facilitates Li wettability and diffusion. Many coatings present good lithiophilicity;[40–44] however, the mechanism is poorly understood.[45] By *in situ* TEM observations on the carbon tubules with ZnO_x, it was revealed that a layer of Li_2O with several nanometers was formed on the MIEC surface during lithiation, and the Li metal underwent a complete wetting to spread along the MIEC surface during deposition. This illustrates that the oxide/Li_2O layer as a strong lithiophilic agent can facilitate the spreading of Li metal on the MIEC surface (Figure 2D).

THERMODYNAMIC MODEL

The 3D porous MIEC/ELI structure is combined with Li metal to form the anode of the all-solid-state battery. Compared with the current 2D Li-foil anodes, the multiple electrochemically engineered interfaces endow the creep-enabled 3D anode with distinct kinetics of Li deposition and stripping. A general thermodynamic model (Figure 4) is introduced here to outline the kinetics.

From the thermodynamic perspective, the chemical potential of Li atom in the Li_{BCC} phase depends on the local composition and stress state,[46,47] as:

$$\mu_{Li}(\mathbf{x}) = \mu_{Li}^{0} + k_B T \ln\gamma_{Li} X_{Li}(\mathbf{x}) + \Omega_{Li\cdot BCC} P_{Li\cdot BCC}(\mathbf{x}) \qquad \text{(Equation 4.1)}$$

where μ_{Li}^{0} is the chemical potential of a Li atom in a Li_{BCC} perfect crystal at a pressure-free condition, k_B is the Boltzmann constant, T is the temperature, γ_{Li} is the activity coefficient of Li element, X_{Li} is the mole fraction, $\Omega_{Li\ BCC}$ is the Li atomic volume, and $P_{Li\ BCC}(\mathbf{x})$ is the pressure on Li metal.

During Li deposition, Li-ions transport through the SE and are neutralized with electrons to form and deposit Li atoms at the SE/Li_{BCC} interface (labeled as "SE/Li interface"). The Li insertion at the SE/Li_{BCC} interface requires extra volume and generates high compressive stress therein. In contrast, on the free surface of Li_{BCC} (labeled as "Li surface"), the pressure is nearly zero. This establishes a pressure difference along the tubule:

$$P_{Li\ BCC}(\text{SE/Li interface}) > P_{Li\ BCC}(\text{Li surface}) = 0$$

This pressure difference corresponds to a difference in the chemical potential of Li_{BCC}:

$$\mu_{Li}\ (\text{SE/Li interface}) > \mu_{Li}\ (\text{Li surface})$$

Please cite this article in press as: Wang et al., Creep-Enabled 3D Solid-State Lithium-Metal Battery, Chem (2020), https://doi.org/10.1016/j.chempr.2020.09.005

Therefore, the Li atoms deposited at the SE/Li interface are driven to flow (i.e., creep) from the SE/Li interface of high compressive stress toward the free surface with zero stress. From this point of view, the terminology of "creep" used in this context should be understood as a "diffusion and deposition" process. That is to say, the Li atoms deposited at the SE/Li interface diffuse under the stress gradient (chemical-potential gradient) and transport to the free surface with lower compressive stress.

The thermodynamic driving force for Li diffusion is the negative gradient of the chemical potential, $-\nabla\mu_{Li}$. The pressure gradient contributes to the chemical potential, $-\Omega_{Li\ BCC}\nabla P_{Li\ BCC}(x)$, and results in a shear stress along the MIEC/Li_{BCC} interface that drives the interfacial diffusion.

At the SE/Li interface, the neutralization charge-transfer reaction between the electrons with an overpotential of Φ and the Li-ions just across the SE can be written as

$$e^{-}(\phi) + Li^{+}(SE) = Li_{BCC}(SE / Li\ interface) \quad \text{(Equation 4.2)}$$

From the balance of the chemical potential, we can obtain

$$\mu_{Li}(SE / Li\ interface) \rightleftharpoons -e\phi + \mu_{Li^{+}} \cdot (SE) \quad \text{(Equation 4.3)}$$

From Equation 4.3, it is seen that if the applied overpotential is reversed at the SE/Li interface, the ionization reaction of Li atoms and Li stripping may occur. During the stripping process, a tensile stress (negative pressure) is generated and applied to Li metal at the SE/Li interface as the Li atoms are ionized:

$$P_{Li\ BCC}(SE/Li\ interface) < P_{Li\ BCC}(Li\ surface) = 0$$

Correspondingly, the chemical potential differs:

$$\mu_{Li}(SE/Li\ interface) < \mu_{Li}(Li\ surface)$$

This shows that the driving force turns to the opposite direction for Li stripping.

According to Fick's first law,[48] the Li atom flux J_{Li} is driven by the chemical-potential gradient,

$$J_{Li}(x) = -MC_{Li}\nabla\mu_{Li}(x) \quad \text{(Equation 4.4)}$$

where M is the mobility of the Li atom ($M=D/k_BT$, and D is the diffusivity), and C_{Li} is the concentration of the Li atom.

CARBONACEOUS POROUS MIEC

To illustrate the design concept, a carbonaceous MIEC tubular structure at cm × cm scale with open pores has been fabricated to test the electrochemical performance.[27] According to the design principles, the MIEC tubules should comply with the following scales: the length h = 10–100 μm to ensure capacity, the inner diameter of tubules W~100 nm to ensure Coble creep, and the tubule wall thickness w~10 nm to ensure mechanical robustness. Upon Li-metal plating in the 1st cycle, the carbonaceous tubule wall is lithiated to form LiC_6 as the MIEC, with a volume expansion less than 10%.[49] The MIEC wall remains stable against Li metal in the following cycles.

Please cite this article in press as: Wang et al., Creep-Enabled 3D Solid-State Lithium-Metal Battery, Chem (2020), https://doi.org/10.1016/j.chempr.2020.09.005

The cm × cm scale sample with the carbonaceous MIEC tubular architecture of the above-specified dimensions was successfully constructed using $\sim 10^{10}$ parallel and capped tubules (Figure 5C). For fabrication, first, chemical vapor deposition (CVD) method was employed to deposit a uniform layer of carbon onto the inner surface of anodic aluminum oxide (AAO). A layer of Pt was then deposited by sputtering onto the bottom side of AAO as the current collector. The AAO was further etched to produce the carbonaceous MIEC tubules, and a 1 nm-thick ZnO layer was deposited onto the surface of carbonaceous tubules by atomic layer deposition (ALD) to enhance lithiophilicity.

The MIEC tubules were capped by a 50-μm-thick PEO-based/LiTFSI polymeric film as the SE. A layer of ~200-nm-thick LiPON was pre-deposited by the sputtering method into the MIEC tubules. LiPON is approximated as an ELI on MIEC roots to bind MIEC walls with the SE. Li-metal foil was used as the counter-electrode for the half-cell test and $LiFePO_4$ as a cathode for the full-cell test.

The performance was tested at 55°C. For the half-cell tests, a large amount of Li metal can be cycled in the MIEC tubules with an areal capacity of 1.5 mAh cm^{-2} and a Coulombic efficiency (CE) of 97.12%. This corresponds to ~9-μm-thick Li metal deposited into the MIEC tubules, considering the matrix porosity of 80%. Furthermore, for the solid-state full cells with $\sim 10^{10}$ MIEC cylinders, starting with only 1× excess Li pre-deposited into the tubules, almost no capacity decay was observed for over 50 cycles at 0.1 C, while an average nominal CE of 99.82% was reached. The full-cell areal capacity was about 1 mAh cm^{-2}, and a gravimetric capacity of ~900 mAh g^{-1} was achieved for the anode. The battery can be further improved, in view of the most recent advance.[39] For example, the cyclability and CE can be further improved by using the SE that is more compatible with Li metal to reduce the possible side reactions.

GENERAL 3D POROUS MIEC ARCHITECTURES

The interfacial diffusion mechanism above supports a wide range of general 3D open porous MIEC architectures. Discussions of the feasibilities are given below concerning the aspects of the MIEC and ELI materials, architectures, sizes, and the lithiophilic coatings (Figure 5A).

MIEC

MIEC materials can be synthesized by lithiating anode materials to below 0 V versus Li^+/Li. These include lithiated carbon (LiC_6), silicon ($Li_{22}Si_5$), aluminum (Li_9Al_4), etc., all of which are thermodynamically stable against Li metal. Considering that Li transport is dominated by the Coble creep along the MIEC/Li_{BCC} interface, materials with appreciable solubility of Li atoms, such as $CuLi_x$, can also be regarded as MIEC. MIEC can even be expanded to bulk-immiscible metals (such as Ni and W) that support some Li solubility at the phase boundary between the metal and Li_{BCC}.

ELI

Materials like BeO and SrF_2, which are electronic and Li-ion insulating and thermodynamically stable against Li_{BCC}, belong to ELIs. In other words, ELIs should have a large band gap, sit on a direct tie-line with Li_{BCC} phase in the equilibrium phase diagram without any intervening phases and with vanishing Li solubility. Based on these criteria, ELI candidates can be screened from ab initio phase diagrams (Pei, K. and Li, J., unpublished data).

Please cite this article in press as: Wang et al., Creep-Enabled 3D Solid-State Lithium-Metal Battery, Chem (2020), https://doi.org/10.1016/j.chempr.2020.09.005

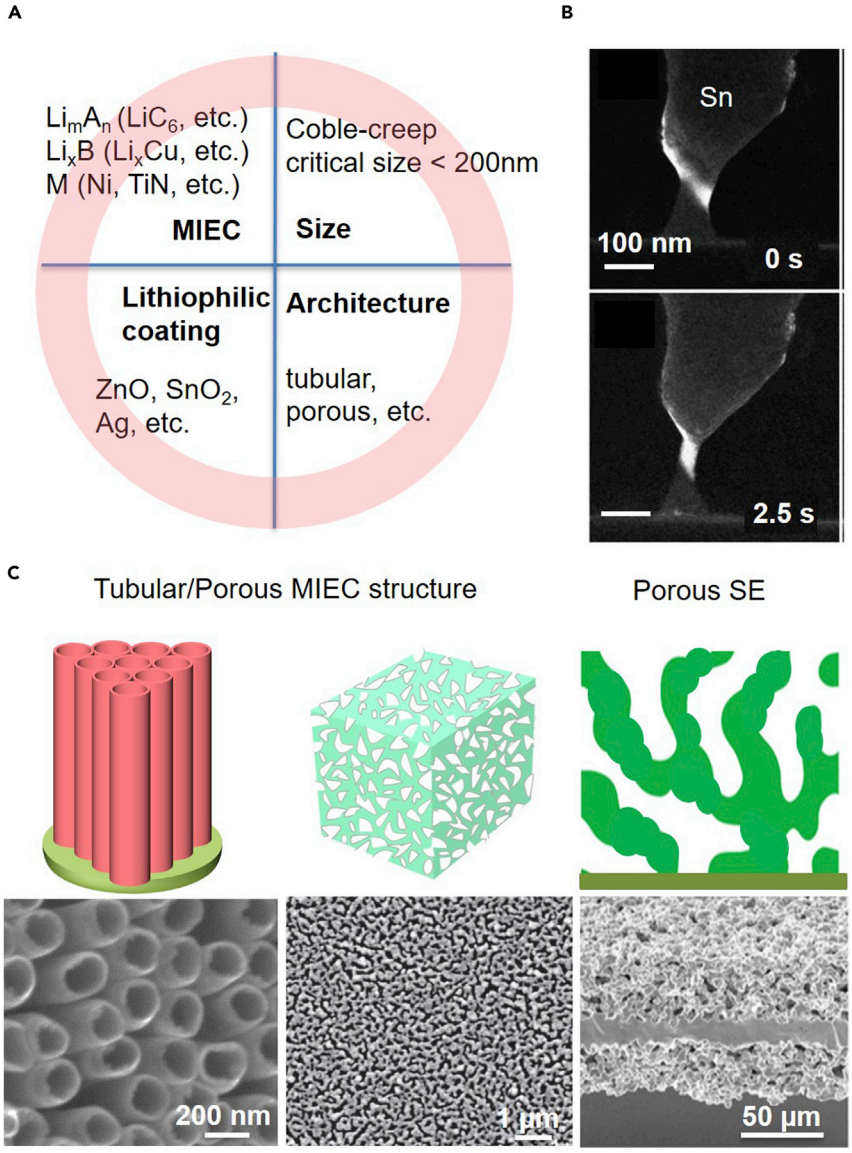

Figure 5. MIEC Architectures

(A) The schematic of the design details with respect to the MIEC materials, architectures, sizes, and the lithiophilic coatings. The formulas of Li_mA_n, Li_xB, and M represent lithiated phase of anodes (LiC_6, $Li_{22}Si_5$, Li_9Al_4, etc.), random solid solution ($CuLi_x$, etc.), and bulk-immiscible material to Li metal (Ni, W, TiN, etc.), respectively.

(B) Dynamic process during the tensile deformation of a Sn_{HCP} nanoligament of ~200 nm size with the final morphology of the ruptured Sn_{HCP} nanoligament turning to the round-shape geometry, implying a Coble creep dominant mechanism. Reprinted with permission from Tian et al.[35] Copyright 2013 Springer Nature.

(C) Examples of the carbonaceous MIEC tubular structure (left), Reprinted with permission from Chen et al.[30] Copyright 2020 Springer Nature; Ni MIEC porous structure (middle), Reprinted with permission from Li et al.[50] Copyright 2018 IOP Science; and a porous structure with Li-ion conductors (right, $Li_5La_3Nb_2O_{12}$ garnet) as Li-metal host, Reprinted with permission from Yang et al.[51] Copyright 2018 National Academy of Sciences.

3D Architecture

In addition to the tubular architecture, 3D porous architectures are also applicable as long as the pores are open-ended, as the diffusive mechanism supports Li metal

Please cite this article in press as: Wang et al., Creep-Enabled 3D Solid-State Lithium-Metal Battery, Chem (2020), https://doi.org/10.1016/j.chempr.2020.09.005

deposition/stripping in the presence of partial internal obstructions or obstacles. To minimize the diffusion distance of Li atoms for increased power density and reduced stress accumulation, porous MIEC hosts with tortuosity τ near 1 are more desirable. But as long as the pores are open end-to-end, with the required opening size < few hundred nm, the concept can work.

Size

The thickness and the porosity of the porous structure determine the maximum available anode capacity. The wall thickness of the porous matrix should not be too thin to ensure mechanical robustness and sustain the perturbation during deposition and stripping. However, there is a critical size for the inner diameter of the porous structures, beyond which diffusional creep (Nabarro-Herring or Coble type) is no longer the dominant mechanism. To estimate the critical size for the diffusional creep of Li metal, we refer to a previous tensile experiment on Sn_{HCP} nano ligaments,[35] since Sn_{HCP} and Li_{BCC} have a similar homologous temperature of $T/T_M \sim 0.6$. It was found from the tensile deformation experiments that, when the size was increased from around 200 to 450 nm, displacive plasticity replaces the diffusional creep as the dominant deformation mechanism (Figure 5B). *In situ* TEM observation confirmed that the Li deposition still proceeds for the MIEC tubule with a diameter of 200 nm. This suggests a critical size of ~200 nm for Coble creep to occur, and ~200–500 nm for Nabarro-Herring creep, for which the stress remains fairly low while yielding a high current density. Above ~500 nm, significant dislocation creep (power-law creep) may occur, which is a hybrid diffusive-displacive mechanism. In this case, the stress can rise up to a very high level, which may endanger the mechanical integrity of the all-solid-state battery.

Initial Lithiophilic Coating

Besides ZnO_x, oxides like MnO_2, Co_3O_4, and SnO_2,[44] and metals like Au, Ag, Zn, and Mg[52] can all present good lithiophilicity. Synthesis techniques, such as ALD, hydrothermal treatment, etc., can be applied to introduce the lithiophilic agents into the 3D porous MIEC structures.

The broad availability of the MIEC, ELI, and lithophilic coating materials offers flexible choices for building the 3D porous host. Indeed, there have already been many 3D porous structures fabricated and reported,[51,53,54] though most of them are used for the Li-metal batteries with liquid electrolytes. As another example[50] for 3D porous MIEC structures, as shown in Figure 5C, a nanoporous Ni film with an average pore width of ~100 nm can be fabricated and can be considered as a 3D porous MIEC structure. A 3D porous framework of Li-ion conductors as the Li-metal host (Figure 5C) has also been reported.[51] In such a case, the Li-metal deposition and stripping may still follow the Coble creep mechanism. The material framework discussed above opens exciting opportunities for building high-performance all-solid-state batteries.

OUTLOOK

Li metal is both electrochemically aggressive and mechanically stressful. Interfacing Li metal with other solid components has become a critical issue, roadblocking the development of safe and high-energy-density all-solid-state Li-metal batteries. These electrochemical and mechanical degradation mechanisms are intimately coupled, making the construction of robust Li-metal anodes quite challenging, both conceptually and practically.

To battle the electrochemomechanical degradations in Li-metal batteries, we have introduced an expanded library of materials, each with its own distinct transport

Please cite this article in press as: Wang et al., Creep-Enabled 3D Solid-State Lithium-Metal Battery, Chem (2020), https://doi.org/10.1016/j.chempr.2020.09.005

properties (M, SE, MIEC, and ELI), offering the complete repertoire for mitigating electrochemomechanical degradation. A novel design concept, involving a 3D open porous architecture made of MIEC and ELI as the Li-metal host, along with Li metal and SE, constitute a complete framework for constructing the battery engine. Various interfaces within the engine can be tuned to simultaneously direct electronic, ionic, and atomic flows with minimized corrosive reactions and stress generations.

When shifting from liquid electrolyte to all-solid-state cells, growth inherent to Li deposition generates huge mechanical stress into the solid components, causing interfacial decohesion, fracture of SE, and Li-dendrite penetration. In liquid cells, such displacement is largely accommodated by the fluidity of the liquid electrolytes, though stress-induced instabilities still occur at the SEI-Li_{BCC} interface.[54] In all-solid-state batteries, all the components are solid and displacive deformation appear to be difficult to evade. Considering Li metal as a soft metal, we innovatively demonstrated that displacive deformation of Li_{BCC} driven by high stress accumulation can be suppressed and low-stress Li diffusion can be activated along the MIEC/Li-metal interface with $\delta_{interface}$ ~2 Å. The resulting diffusional creep effectively alleviates mechanical stress[51,55] during Li deposition and stripping. This further demonstrates the importance of interfacial engineering through both expanding the materials classes (M, SE, MIEC, and ELI) exploited, and the selection of materials (MIEC and ELI) that are absolutely thermodynamically phase stable against Li_{BCC} in the voltage range considered.

Though the present design concept is developed for Li-metal batteries, it is readily applicable to the other alkali-metal battery systems. Indeed, reversible Na_{BCC} deposition and stripping in MIEC tubules have been demonstrated by *in situ* TEM. In the same spirit of engineering appropriate interfaces using the orthogonal transport properties of materials, this design concept can be further extended to construct the battery engines with liquid or gel electrolytes or other concomitant diffusing elements like Ag.[39] As demonstrated in the 3D porous architecture, an essential component of the design in this extension is to engineer the material interfaces and selectively direct electronic, ionic, and atomic flows along the materials interfaces, thereby minimizing detrimental side reactions and creating effective stress relaxation channels, for enhancing shape fluidity by nanostructuring.[17,56]

For the practical productions of creep-enabled 3D solid-state Li-metal batteries, further optimizations on the full-cell level, including the cathode, SE, and anode, are necessary. The high-capacity cathode like $LiNi_{0.90}Co_{0.05}Mn_{0.05}O_2$ (NMC) with a large areal loading can be used to increase the cell energy density. Both sulfide and oxide SEs[5,29] with high Li-ion conductivities are suitable for the preparation of cells with excellent rate capability. Sulfide SE is soft, and the MIEC/SE interfacial contact can be enhanced by simple mechanical pressing, but controlled chemical conditions are needed to prepare the environmentally sensitive sulfide SE. Garnet-type oxide SE manifests better compatibility against Li metal. But oxide SE is mechanically brittle. Thus, mechanically compliant but thin polymer SE layer may be added onto the brittle oxide SE layer via a method like dip coating, to enable the intimate interfacial contact between SE and MIEC upon pressing. With further optimizations,[39,57] the Li-free anode (i.e., porous MIEC matrix with zero Li-metal inventory) can be achieved for the practical cell.[39] The production of carbonaceous MIEC porous structures on a large scale could also be achieved through an approach like the thermal decompositions of 3D cross-linked copolymers or via a technique like the multinozzle electrospinning[57] to produce the porous matrix of carbon hollow

Please cite this article in press as: Wang et al., Creep-Enabled 3D Solid-State Lithium-Metal Battery, Chem (2020), https://doi.org/10.1016/j.chempr.2020.09.005

tubules. With those practical low-cost and viable approaches for further optimizations, we estimate that a practical pouch cell of the creep-enabled 3D solid-state Li-metal battery can attain a gravimetric energy density of over 500 Wh kg^{-1} and a volumetric energy density over 800 Wh L^{-1}.

Future development and optimization hinge upon expanding the material space and refined interfacial engineering of the 3D open porous structure. For example, the cycling stability can be further increased by identifying MIEC/ELI/SE combinations to strengthen the MIEC/ELI and ELI/SE interfaces. In particular, a better lithiophobic ELI can be used to protect the ELI/SE binding interfaces from decohesion by Li flooding, and a better lithiophilic coating onto the MIEC walls can be used to enhance Li-metal infusion and diffusion. In addition to the material selection and interfacial engineering, dimensional and architecture designs, which can be further invoked to minimize Li meal/SE interface for reduced SEI formation and maximally activate Li atom diffusion through Coble creep, are also essential to improve the battery performance. Finally, innovative fabrication approaches are yet to be developed to scale up the nanoscale design in a cost-effective manner.

ACKNOWLEDGMENTS

This work is financially supported by the Samsung Advanced Institute of Technology. X.Y.L. would like to acknowledge the support by the Award Program for Minjiang Scholar Professorship. S.L.Z. acknowledges support by NSF CBET-2034899.

AUTHOR CONTRIBUTIONS

Z.W., X.L., Y.C., S.Z., and J.L. conceived and wrote the manuscript. Y.-W.M. and K.P. discussed and edited the manuscript.

REFERENCES

1. Janek, J., and Zeier, W.G. (2016). A solid future for battery development. Nat. Energy *1*, 16141.
2. Suo, L., Xue, W., Gobet, M., Greenbaum, S.G., Wang, C., Chen, Y., Yang, W., Li, Y., and Li, J. (2018). Fluorine-donating electrolytes enable highly reversible 5-V-class Li metal batteries. Proc. Natl. Acad. Sci. USA *115*, 1156–1161.
3. Inoue, T., and Mukai, K. (2017). Are all-solid-state lithium-ion batteries really safe?-Verification by differential scanning calorimetry with an all-inclusive microcell. ACS Appl. Mater. Interfaces *9*, 1507–1515.
4. Li, J., Ma, C., Chi, M., Liang, C., and Dudney, N.J. (2015). Solid electrolyte: the key for high-voltage lithium batteries. Adv. Energy Mater. *5*, 1401408.
5. Kato, Y., Hori, S., Saito, T., Suzuki, K., Hirayama, M., Mitsui, A., Yonemura, M., Iba, H., and Kanno, R. (2016). High-power all-solid-state batteries using sulfide superionic conductors. Nat. Energy *1*, 16030.
6. Armstrong, R.D., Dickinson, T., and Turner, J. (1974). The breakdown of β-alumina ceramic electrolyte. Electrochim. Acta *19*, 187–192.
7. Monroe, C., and Newman, J. (2005). The impact of elastic deformation on deposition kinetics at lithium/polymer interfaces. J. Electrochem. Soc. *152*, A396–A404.
8. Lukas, P., Swamy, T., Sheldon, B., Rettenwander, D., Frömling, T., Thaman, H., Berendts, S., Uecker, R., Carter, W.C., and Chiang, Y.-M. (2017). Mechanism of lithium metal penetration through inorganic solid electrolytes. Adv. Energy Mater. *7*, 1701003.
9. Zhang, L., Yang, T., Du, C., Liu, Q., Tang, Y., Zhao, J., Wang, B., Chen, T., Sun, Y., Jia, P., et al. (2020). Lithium whisker growth and stress generation in an in situ atomic force microscope–environmental transmission electron microscope set-up. Nat. Nanotechnol. *15*, 94–98.
10. Ren, Y., Shen, Y., Lin, Y., and Nan, C.W. (2015). Direct observation of lithium dendrites inside garnet-type lithium-ion solid electrolyte. Electrochem. Commun. *57*, 27–30.
11. Suzuki, Y., Kami, K., Watanabe, K., Watanabe, A., Saito, N., Ohnishi, T., Takada, K., Sudo, R., and Imanishi, N. (2015). Transparent cubic garnet-type solid electrolyte of Al2O3-doped Li7La3Zr2O12. Solid State Ion *278*, 172–176.
12. Sudo, R., Nakata, Y., Ishiguro, K., Matsui, M., Hirano, A., Takeda, Y., Yamamoto, O., and Imanishi, N. (2014). Interface behavior between garnet-type lithium-conducting solid electrolyte and lithium metal. Solid State Ion *262*, 151–154.
13. Cheng, E.J., Sharafi, A., and Sakamoto, J. (2017). Intergranular Li metal propagation through polycrystalline Li6.25Al0.25La3Zr2O12 ceramic electrolyte. Electrochim. Acta *223*, 85–91.
14. Ni, J.E., Case, E.D., Sakamoto, J.S., Rangasamy, E., and Wolfenstine, J.B. (2012). Room temperature elastic moduli and Vickers hardness of hot-pressed LLZO cubic garnet. J. Mater. Sci. *47*, 7978–7985.
15. Ferrese, A., and Newman, J. (2014). Mechanical deformation of a lithium-metal anode due to a very stiff separator. J. Electrochem. Soc. *161*, A1350–A1359.
16. Zhu, T., and Li, J. (2010). Ultra-strength materials. Prog. Mater. Sci. *55*, 710–757.
17. Sun, J., He, L., Lo, Y.C., Xu, T., Bi, H., Sun, L., Zhang, Z., Mao, S.X., and Li, J. (2014). Liquid-like pseudoelasticity of sub-10-nm crystalline silver particles. Nat. Mater. *13*, 1007–1012.
18. Guo, W., Wang, Z., and Li, J. (2015). Diffusive versus displacive contact plasticity of nanoscale asperities: temperature- and velocity-dependent strongest size. Nano Lett *15*, 6582–6585.
19. Richards, W.D., Miara, L.J., Wang, Y., Kim, J.C., and Ceder, G. (2016). Interface stability in solid-state batteries. Chem. Mater. *28*, 266–273.
20. Zhang, W., Schröder, D., Arlt, T., Manke, I., Koerver, R., Pinedo, R., Weber, D.A., Sann, J., Zeier, W.G., and Janek, J. (2017). (Electro) chemical expansion during cycling: monitoring the pressure changes in operating solid-state lithium batteries. J. Mater. Chem. A *5*, 9929–9936.

21. Koerver, R., Zhang, W., de Biasi, L., Schweidler, S., Kondrakov, A.O., Kolling, S., Brezesinski, T., Hartmann, P., Zeier, W.G., and Janek, J. (2018). Chemo-mechanical expansion of lithium electrode materials – on the route to mechanically optimized all-solid-state batteries. Energy Environ. Sci. *11*, 2142–2158.

22. Koerver, R., Aygün, I., Leichtweiß, T., Dietrich, C., Zhang, W., Binder, J.O., Hartmann, P., Zeier, W.G., and Janek, J. (2017). Capacity fade in solid-state batteries: interphase formation and chemomechanical processes in nickel-rich layered oxide cathodes and lithium thiophosphate solid electrolytes. Chem. Mater. *29*, 5574–5582.

23. Bucci, G., Talamini, B., Renuka Balakrishna, A., Chiang, Y.-M., and Carter, W.C. (2018). Mechanical instability of electrode–electrolyte interfaces in solid-state batteries. Phys. Rev. Materials *2*, 105407.

24. Devaux, D., Harry, K.J., Parkinson, D.Y., Yuan, R., Hallinan, D.T., MacDowell, A.A., and Balsara, N.P. (2015). Failure mode of lithium metal batteries with a block copolymer electrolyte analyzed by X-ray microtomography. J. Electrochem. Soc. *162*, A1301–A1309.

25. Maslyn, J.A., Loo, W.S., McEntush, K.D., Oh, H.J., Harry, K.J., Parkinson, D.Y., and Balsara, N.P. (2018). Growth of lithium dendrites and globules through a solid block copolymer electrolyte as a function of current density. J. Phys. Chem. C *122*, 26797–26804.

26. Harry, K.J., Liao, X., Parkinson, D.Y., Minor, A.M., and Balsara, N.P. (2015). Electrochemical deposition and stripping behavior of lithium metal across a rigid block copolymer electrolyte membrane. J. Electrochem. Soc. *162*, A2699–A2706.

27. Sharafi, A., Kazyak, E., Davis, A.L., Yu, S., Thompson, T., Siegel, D.J., Dasgupta, N.P., and Sakamoto, J. (2017). Surface chemistry mechanism of ultra-low interfacial resistance in the solid-state electrolyte Li7La3Zr2O12. Chem. Mater. *29*, 7961–7968.

28. Hitz, G.T., McOwen, D.W., Zhang, L., Ma, Z., Fu, Z., Wen, Y., Gong, Y., Dai, J., Hamann, T.R., Hu, L., and Wachsman, E.D. (2019). High-rate lithium cycling in a scalable trilayer Li-garnet-electrolyte architecture. Mater. Today *22*, 50–57.

29. Han, X., Gong, Y., Fu, K.K., He, X., Hitz, G.T., Dai, J., Pearse, A., Liu, B., Wang, H., Rubloff, G., et al. (2017). Negating interfacial impedance in garnet-based solid-state Li metal batteries. Nat. Mater. *16*, 572–579.

30. Chen, Y., Wang, Z., Li, X., Yao, X., Wang, C., Li, Y., Xue, W., Yu, D., Kim, S.Y., Yang, F., et al. (2020). Li metal deposition and stripping in a solid-state battery via Coble creep. Nature *578*, 251–255.

31. Jin, C., Sheng, O., Luo, J., Yuan, H., Fang, C., Zhang, W., Huang, H., Gan, Y., Xia, Y., Liang, C., et al. (2017). 3D lithium metal embedded within lithiophilic porous matrix for stable lithium metal batteries. Nano Energy *37*, 177–186.

32. Zhao, J., Zhou, G., Yan, K., Xie, J., Li, Y., Liao, L., Jin, Y., Liu, K., Hsu, P.-C., Wang, J., et al. (2017). Air-stable and freestanding lithium alloy/graphene foil as an alternative to lithium metal anodes. Nat. Nanotechnol. *12*, 993–999.

33. Frost, H., and Ashby, M. (1982). Deformation-Mechanism Maps (Pergamon Press).

34. Tu, K.N. (2007). Spontaneous tin whisker growth: mechanism and prevention. In Solder Joint Technology - Materials, Properties, and Reliability (Springer Nature)), pp. 153–181.

35. Tian, L., Li, J., Sun, J., Ma, E., and Shan, Z.W. (2013). Visualizing size-dependent deformation mechanism transition in Sn. Sci. Rep. *3*, 2113.

36. Herring, C. (1950). Diffusional viscosity of a polycrystalline solid. J. Appl. Phys. *21*, 437–445.

37. Mali, M., Roos, J., Sonderegger, M., Brinkmann, D., and Heitjans, P. (1988). 6Li and 7Li diffusion coefficients in solid lithium measured by the NMR pulsed field gradient technique. J. Phys. F: Met. Phys. *18*, 403–412.

38. Gjostein, N.A. (1973) (Diffusion: ASM Press), pp. 241–274.

39. Lee, Y., Fujiki, S., Jung, C., Suzuki, N., Yashiro, N., Omoda, R., Ko, D., Shiratsuchi, T., Sugimoto, T., Ryu, S., et al. (2020). High-energy long-cycling all-solid-state lithium metal batteries enabled by silver–carbon composite anodes. Nat. Energy *5*, 299–308.

40. Park, M.G., Sung, G., Sung, N., Kim, J., and Park, C. (2016). Partially reversible Li2O formation in ZnO: a critical finding supporting realization of highly reversible metal oxide electrodes. J. Power Sources *328*, 607–614.

41. Reddy, M.V., Subba Rao, G.V., and Chowdari, B.V.R. (2013). Metal oxides and oxysalts as anode materials for Li ion batteries. Chem. Rev. *113*, 5364–5457.

42. Zhang, Z., Xu, X., Wang, S., Peng, Z., Liu, M., Zhou, J., Shen, C., and Wang, D. (2016). Li2O-reinforced Cu nanoclusters as porous structure for dendrite-free and long-lifespan lithium metal anode. ACS Appl. Mater. Interfaces *8*, 26801–26808.

43. Liu, Y., Lin, D., Liang, Z., Zhao, J., Yan, K., and Cui, Y. (2016). Lithium-coated polymeric matrix as a minimum volume-change and dendrite-free lithium metal anode. Nat. Commun. *7*, 10992.

44. Yu, B., Tao, T., Mateti, S., Lu, S., and Chen, Y. (2018). Nanoflake arrays of Lithiophilic metal oxides for the ultra-stable anodes of lithium-metal batteries. Adv. Funct. Mater. *28*, 1803023.

45. Duan, J., Zheng, Y., Luo, W., Wu, W.Y., Wang, T.R., Xie, Y., Li, S., Li, J., and Huang, Y.H. (2020). Is graphite lithiophobic or lithiophilic? Natl Sci. Rev. *7*, 1208–1217.

46. Kim, S., Choi, S.J., Zhao, K.J., Yang, H., Gobbi, G., Zhang, S.L., and Li, J. (2016). Electrochemically driven mechanical energy harvesting. Nat. Commun. *7*, 10146.

47. Xue, W.J., Chen, T.W., Ren, Z.C., Kim, S.Y., Chen, Y.M., Zhang, P.P., Zhang, S.L., and Li, J. (2020). Molar-volume asymmetry enabled low-frequency mechanical energy harvesting in electrochemical cells. Appl. Energy *273*, 115230.

48. Fick, A. (1855). On liquid diffusion. Ann. Physik Chem. *94*, 59.

49. Shellikeri, A., Watson, V., Adams, D., Kalu, E.E., Read, J.A., Jow, T.R., Zheng, J.S., and Zheng, J.P. (2017). Investigation of pre-lithiation in graphite and hard-carbon anodes using different lithium source structures. J. Electrochem. Soc. *164*, A3914–A3924.

50. Li, C., Wang, M., Luo, Q., and Kim, E.J. (2018). Nanoporous nickel films on glass substrate by sol–gel technique. Mater. Res. Express *5*, 7.

51. Yang, C., Zhang, L., Liu, B., Xu, S., Hamann, T., McOwen, D., Dai, J., Luo, W., Gong, Y., Wachsman, E.D., and Hu, L. (2018). Continuous plating/stripping behavior of solid-state lithium metal anode in a 3D ion-conductive framework. Proc. Natl. Acad. Sci. USA *115*, 3770–3775.

52. Yan, K., Lu, Z., Lee, H., Xiong, F., Hsu, P., Li, Y., Zhao, J., Chu, S., and Cui, Y. (2016). Selective deposition and stable encapsulation of lithium through heterogeneous seeded growth. Nat. Energy *1*, 16010.

53. Erlebacher, J., Aziz, M.J., Karma, A., Dimitrov, N., and Sieradzki, K. (2001). Evolution of nanoporosity in dealloying. Nature *410*, 450–453.

54. Li, S., Jiang, M., Xie, Y., Xu, H., Jia, J., and Li, J. (2018). Developing high-performance lithium metal anode in liquid electrolytes: challenges and progress. Adv. Mater. *30*, e1706375.

55. Yan, P., Zheng, J., Chen, T., Luo, L., Jiang, Y., Wang, K., Sui, M., Zhang, J.G., Zhang, S., and Wang, C. (2018). Coupling of electrochemically triggered thermal and mechanical effects to aggravate failure in a layered cathode. Nat. Commun. *9*, 2437.

56. Shishvan, S.S., McMeeking, R.M., Pollock, T.M., and Deshpande, V.S. (2017). Discrete dislocation plasticity analysis of the effect of interfacial diffusion on the creep response of Ni single-crystal superalloys. Acta Mater *135*, 188–200.

57. Li, X., Chen, W., Qian, Q., Huang, H., Chen, Y., Wang, Z., Chen, Q., Yang, J., Li, J., and Mai, Y. (2020). Electrospinning-based strategies for battery materials. Adv. Energy Mater. https://doi.org/10.1002/aenm.202000845.